THE JOURNAL OF PHYSICAL CHEMISTRY B
A JOURNAL OF THE AMERICAN CHEMICAL SOCIETY

pubs.acs.org/JPCB

Article

Long-Wavelength Fluctuations in Quasi-2D Supercooled Liquids

Published as part of The Journal of Physical Chemistry virtual special issue "Pablo G. Debenedetti Festschrift".

Ryan C. Roberts, Jeremy C. Palmer,* and Jacinta C. Conrad*

Cite This: *J. Phys. Chem. B* 2023, 127, 961−969

Read Online

ACCESS | Metrics & More | Article Recommendations

ABSTRACT: We use molecular simulation to characterize the dynamics of supercooled liquids confined in quasi-2D slit geometries. Similar to bulk supercooled liquids, the confined systems exhibit subdiffusive dynamics on intermediate time scales arising from particle localization inside their neighbor cages, followed by an eventual crossover to diffusive behavior as cage rearrangement occurs. The quasi-2D confined liquids also exhibit signatures of long-wavelength fluctuations (LWFs) in the lateral directions parallel to the confining walls, reminiscent of the collective displacements observed in 2D but not 3D systems. The magnitude of the LWFs increases with the lateral dimensions of systems with the same particle volume fraction and confinement length scale, consistent with the logarithmic scaling predicted for 2D Mermin-Wagner fluctuations. The amplitude of the fluctuations is a nonmonotonic function of the confinement length scale because of a competition between caging and strengthening LWFs upon approaching the 2D limit. Our findings suggest that LWFs may play an important role in understanding the behavior of confined supercooled liquids due to their prevalence over a surprisingly broad range of particle densities and confinement length scales.

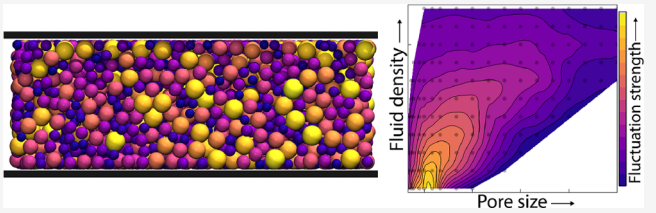

INTRODUCTION

Strongly confined fluids exhibit properties that are distinct from those observed in bulk systems. For example, in a variety of fluids, including gases,[1,2] liquids,[3,4] polymers,[5−7] and colloidal suspensions,[8,9] confinement has been shown to induce solid-like behavior that strengthens as the characteristic confinement length scale is decreased. There remains significant interest in understanding how the properties of fluids change as they are confined from three toward two dimensions, with practical relevance in applications ranging from separations and porous media characterization to energy storage and production and materials synthesis.[1,2,10−14]

The crossover from two to three dimensions has been extensively explored for one prototypical supercooled liquid, a concentrated suspension of nearly hard spheres. When confined in a quasi-2D slit geometry, in which the height of the slit is much smaller than its lateral dimensions, uniformly sized particles form layers at the walls[15,16] and arrange into a variety of ordered crystal structures.[17,18] Although introducing size dispersity can frustrate long-range crystalline ordering,[19,20] these systems can still undergo a transition to a disordered solid-like phase, in which the particle dynamics become increasingly slow and eventually arrest, upon increasing confinement. This transition is reminiscent of the 3D glass transition, in which the viscosity dramatically increases as the liquid is cooled. The dynamical signature of the 3D glass transition is the emergence of a plateau in translational correlation functions, signaling the formation of transient local cages that constrain particle motions. This plateau extends to longer times as the temperature is decreased or the particle concentration is increased.[8,21,22]

Liquids in 2D and 3D exhibit different dynamics[23] and phase behavior, however, complicating understanding of the relationship between the 2D and 3D glass transitions. In 2D, the crystal phase is unstable in the thermodynamic limit due to long-wavelength Mermin-Wagner (MW) fluctuations that represent elastic modes.[24−26] Evidence of MW fluctuations has been recently found in both 2D liquids[27] and amorphous solids.[28] For 2D supercooled liquids, MW fluctuations disrupt particle cages and enable particles to become delocalized.[23,29−31] Thus, 2D supercooled liquids exhibit distinct dynamics from their 3D counterparts.[23,29] However, as shown in experiments[28,31,32] and simulations,[27,30,33,34] the behavior in 2D and 3D systems is similar when particle motions are characterized relative to the cages formed by their nearest neighbors.[30,33,34] These studies suggest that analysis of the cage-relative motions of particles can be used to investigate the behavior of confined supercooled liquids as the dimensionality

Received: October 23, 2022
Revised: December 15, 2022
Published: January 19, 2023

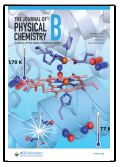

https://doi.org/10.1021/acs.jpcb.2c07417
J. Phys. Chem. B 2023, 127, 961−969

continuously changes from 2D to 3D, which remains incompletely understood.[35]

Here, we use molecular dynamics (MD) simulations to show that quasi-2D supercooled liquid systems of particles confined in slits exhibit long-wavelength fluctuations (LWFs) analogous to those previously observed in dense monolayers. The magnitude of collective particle displacements in the lateral directions parallel to the confining walls, obtained by removing the cage-relative contribution to the mean-square displacement, increases with system size, consistent with the logarithmic growth expected for MW fluctuations. Both the amplitude of the fluctuations and the scaling constant depend nonmonotonically on the confinement length scale, which we attribute to a competition between arrest-driven caging and strengthening LWFs as the 2D limit is approached. These results indicate that dynamics in confined quasi-2D supercooled liquids are affected by steric effects and LWFs.

METHODS

Simulations. We used event-driven molecular dynamics (MD)[19,20,36] to simulate N = 6912−42 592 hard spheres confined in a slit geometry, consisting of two repulsive parallel walls separated by a distance W along the z-axis of the simulation cell (Figure 1(a)). The walls have edge lengths of L along the x- and y-axes of the cell, and periodic boundary conditions are imposed in these directions to model an infinite slab. The particles have unit mass m = 1 and are polydisperse in size (ca. 23%) to prevent spontaneous crystallization. Polydispersity was introduced by assigning each particle a diameter σ randomly drawn from the distribution $P(\sigma_i) = A/\sigma_i^3$ with $\sigma_i \in [0.7255, 1.609]$ (Figure 1(b)), yielding an average size of $\overline{\sigma}$ = 1. Following convention, we adopt a system of reduced units to describe the systems and our results, in which Boltzmann's constant k_B = 1, and $\overline{\sigma}$ and $\tau = \overline{\sigma}(m/k_BT)^{1/2}$ are the fundamental measures of length and time, respectively, where T is the temperature.[19] We define the confinement parameter $H = W - \overline{\sigma}$ based on the width of the slit geometry accessible to an average-sized particle; the volume fraction $\phi = N\pi\overline{\sigma}^3/6WL^2$ is defined in terms of W.

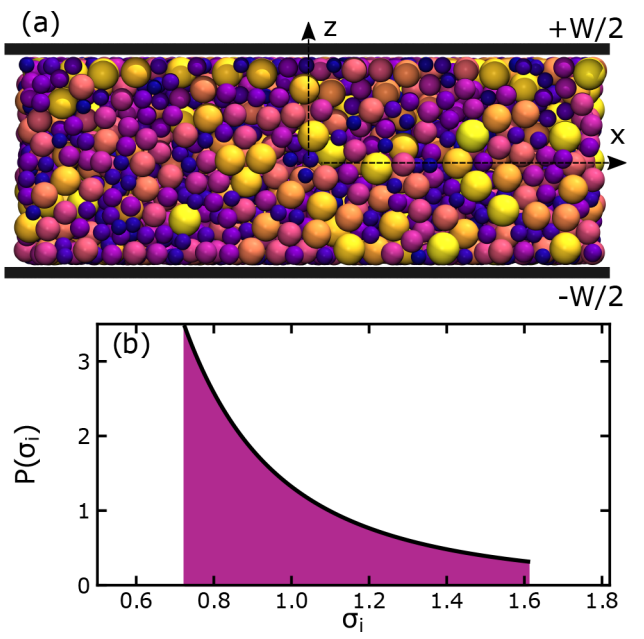

Figure 1. (a) Confined hard-sphere supercooled liquid system with $\{\phi, H\} = \{0.57, 9.00\}$. The walls of the slit geometry are rendered as black rectangles, and the particles are represented as spheres shaded based on their diameter (small to large using a purple to yellow color scale). (b) Probability distribution of the particle diameter σ_i, selected from the distribution $P(\sigma_i) = A/\sigma_i^3$ with $\sigma_i \in [0.7255, 1.6099]$ such that the average size $\overline{\sigma}$ = 1.

Initial particle configurations were generated by gradually compressing a system with ϕ = 0.45, in increments of $\Delta\phi$ = 0.01, to achieve the final targeted ϕ and H. After each incremental compression step, stress in the system was relaxed using MD and/or swap Monte Carlo (SMC).[37−39] In most cases, stress relaxation was achieved by a running short MD simulation 10 time units in duration. For very confined or dense systems, relaxation following each of the last few compression steps was achieved by performing 10^5 sweeps with the SMC algorithm, where 1 sweep is N attempted MC moves. Following compression, the systems were equilibrated using SMC, performing enough MC sweeps (10^5−10^9) to ensure that the particles moved at least twice the mean particle diameter on average. The final equilibrated configurations from the SMC simulations were used to propagate microcanonical (NVE) MD trajectories 10^2−10^4 time units in duration for the analysis of dynamics. Initial particle momenta in the MD simulations were randomly sampled from the Maxwell−Boltzmann distribution specified by T = 1. Dynamical quantities and associated statistical uncertainties were estimated from the averages and standard errors, respectively, computed from MD trajectories propagated from 50 independent realizations of the system at each state point using the protocols described above. Thus, approximately 50 000 simulations in total were performed for this study.

Mean-Square Displacements. From the trajectories, we characterize lateral positional fluctuations in the plane parallel to the walls using the mean-square displacement (MSD),

$$M(t) = \frac{1}{N}\sum_{i=1}^{N} \langle |\delta \mathbf{r}_i(t)|^2 \rangle \tag{1}$$

where $\delta\mathbf{r}_i(t) = \mathbf{r}_i(t) - \mathbf{r}_i(0)$, $\mathbf{r}_i = \{x_i, y_i\}$ is the position of particle i, t is the observation time, and the brackets $\langle\cdots\rangle$ indicate an average over different observation windows.

The cage-relative MSD $M^{CR}(t)$ characterizes the mean-square displacement of a particle relative to the motion of the cage formed by its nearest neighbors and is defined as

$$M^{CR}(t) = \frac{1}{N}\sum_{i}^{N} \langle [\delta \mathbf{r}_i^{CR}(t)]^2 \rangle \tag{2}$$

where

$$\delta \mathbf{r}_i^{CR}(t) = [\mathbf{r}_i(t) - \mathbf{r}_i(0)] - \frac{1}{N_{nn}(i)}\sum_{n=1}^{N_{nn}(i)} [\mathbf{r}_n(t) - \mathbf{r}_n(0)] \tag{3}$$

and $N_{nn}(i)$ indexes the nearest neighbors that form the cage for particle i.

Finally, the effects of LWFs can be analyzed by removing the contributions from cage-rattling from $M(t)$:

$$\Gamma(t) = M(t) - M^{CR}(t) \tag{4}$$

Neighbor Identification. Evaluation of the cage-relative MSD using eqs 2 and 3 requires identifying particles that form

https://doi.org/10.1021/acs.jpcb.2c07417
J. Phys. Chem. B 2023, 127, 961−969

the local neighbor cages. To account for the strong polydispersity, neighbors were identified using the surface-to-surface distance

$$s_{ij} = |\mathbf{x}_i - \mathbf{x}_j| - \frac{\sigma_i + \sigma_j}{2} \tag{5}$$

where $\mathbf{x}_i = \{x_i, y_i, z_i\}$. Two particles were considered to be neighbors if $s_{ij} \leq 0.5$; this value corresponds to approximately the first minimum in the probability density distribution of s_{ij}.

Dynamical Corrections. For some liquid-like systems, we used a modified version of eq 4:

$$\Gamma(t) = M(t) - M^{\mathrm{CR}}(t) - \Delta\gamma_{\mathrm{DD}}(t) - \Delta\gamma_{\mathrm{CB}}(t) \tag{6}$$

where $\Delta\gamma_{\mathrm{DD}}(t)$ and $\Delta\gamma_{\mathrm{CB}}(t)$ are corrections accounting for the asymptotic decorrelation of particle displacements at long times and local rearrangements of neighboring particles at intermediate times, respectively.[29,34] These corrections are needed when the time scales associated with LWFs and the α-relaxation (t_{LWF} and t_α, respectively) are of similar order. For the systems considered here, $t_{\mathrm{LWF}} \approx 10^1 - 10^2$ time units. Thus, we use the criterion $t_\alpha \lesssim 10^2 t_{\mathrm{LWF}} \approx 10^4$ time units as an indicator that these corrections may be necessary, employing an operational definition for t_α as the time required for particles to displace one diameter on average (i.e., $M(t_\alpha) = \bar{\sigma}^2$). For many of our systems, we note that t_α moves outside the accessible window for MD simulations, indicating that these systems are effectively glasses on these time scales and preventing characterization of the terminal relaxation behavior.

For liquids, the long-time behavior of M^{CR} is given by

$$M^{\mathrm{CR}}(t) = M(t) + \langle N_{\mathrm{nn}}(i)\rangle^{-1} M(t) \tag{7}$$

implying that $M^{\mathrm{CR}}(t) > M(t)$. This behavior arises because the displacements of particles become uncorrelated from those of other particles in liquids on long times.[29] For systems where $M^{\mathrm{CR}}(t) > M(t)$, we follow ref 29 and fit the long-time behavior of $M^{\mathrm{CR}}(t)$ and $M(t)$ to power-law functions of the form $Ct^a + b$, where C, a, and b are fitting parameters and a is globally fit for systems of constant ϕ and H. The correction for displacement decorrelation accounts for differences in the long-time growth of $M^{\mathrm{CR}}(t)$ and $M(t)$ and is given by

$$\Delta\gamma_{\mathrm{DD}}(t) = (C_{M^{\mathrm{CR}}} - C_M)t^a \tag{8}$$

Similarly, power-law growth of particle displacements at intermediate times can arise from local rearrangements in neighboring particles, which is not accounted for in the definition of $M^{\mathrm{CR}}(t)$. We correct for this behavior using[29,34]

$$\Delta\gamma_{\mathrm{CB}}(t) = Dt^e \tag{9}$$

where D and $e < 1$ are constants found by fitting the function obtained after correcting for displacement decorrelation.

Correlated Displacements. Correlations between the displacements of particles and those of their surrounding neighbors were quantified using

$$S_{\mathrm{vec},i}(t) = \frac{1}{N_{\mathrm{nn}}(i)} \sum_{j=1}^{N_{\mathrm{nn}}(i)} \frac{\delta\mathbf{r}_i(t)\cdot\delta\mathbf{r}_j(t)}{\max[|\delta\mathbf{r}_i(t)|^2, |\delta\mathbf{r}_j(t)|^2]}. \tag{10}$$

This function is a modified, particle-resolved version of the spatial–temporal correlation function used in refs 32, 40, and 41. The maximum operation in the denominator ensures $-1 \leq S_{\mathrm{vec},i} \leq 1$ and that very small or large neighbor displacements are not disproportionately weighted. The function assumes values of 1 and −1 when the displacement of the central particle i is perfectly correlated and anticorrelated with the displacements of its surrounding neighbors, respectively. Nearest neighbors were identified using the same surface-to-surface distance criterion used in the evaluation of M^{CR}.

To facilitate visualization, we coarse-grained the displacement vector correlation function into a continuous field using Gaussian functions centered at the location of each particle:

$$S_{\mathrm{vec}}(t, x, y) = \sum_{i=1}^{N_{\mathrm{cl}}} S_{\mathrm{vec},i}(t) \mathrm{e}^{\frac{-[(x-x_i)^2+(y-y_i)^2]/\bar{\sigma}^2}{2|\delta\mathbf{r}_i(t)|^2/M(t)}} \tag{11}$$

where the sum is taken over the N_{cl} particles in the contact layer near the lower wall.

RESULTS AND DISCUSSION

Dynamics of Confined Supercooled Liquids. We analyze the dynamics of hard-sphere supercooled liquids confined in a quasi-2D slit geometry. The state of the systems is nominally specified by $\{\phi, H\}$. We study ranges of these parameters ($0.550 \leq \phi \leq 0.600$ and $1.0 \leq H \leq 14.0$) corresponding to high to moderately confined dense packings of particles that exhibit glassy dynamics.

The MSDs for a moderately confined system ($H = 3.00$) illustrate typical behaviors of a supercooled liquid (Figure 2(a)). At volume fraction $\phi = 0.560$, the MSD exhibits ballistic behavior on short time scales, subdiffusive behavior (power-

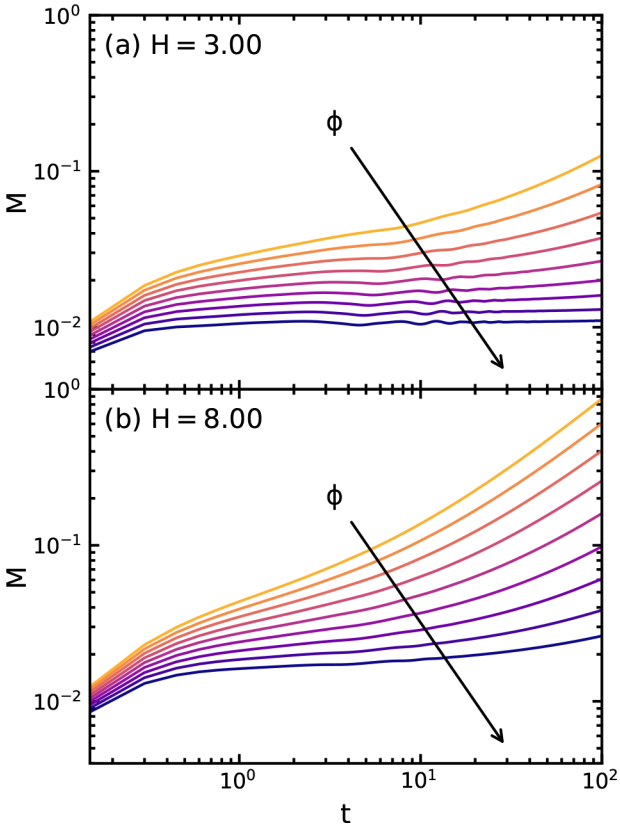

Figure 2. Mean-square displacement $M(t)$ functions for systems with various particle volume fractions $\phi = 0.560$–0.600 and confinement parameters (a) $H = 3.00$ and (b) $H = 8.00$. The arrow indicates the direction of increasing ϕ in steps of $\Delta\phi = 0.005$.

https://doi.org/10.1021/acs.jpcb.2c07417
J. Phys. Chem. B 2023, 127, 961−969

law scaling such that $M(t) \approx t^{\alpha}$ with $\alpha < 1$) on intermediate time scales ($t \approx 1-10$), and an upturn ($t \approx 10$) and gradual crossover to diffusive scaling ($M(t) \approx t$) on long times ($t > 10$). These features are common in dense particle suspensions and deeply supercooled liquids. The subdiffusive behavior at intermediate times arises from "cage-rattling", in which particles are localized inside the cages formed by their surrounding neighbors. The upturn observed for liquid but not glassy samples indicates the onset of local rearrangements that eventually accumulate and allow particles to escape the cages formed by their neighbors.[34] Cage escape is associated with the α- (or terminal-) relaxation process in the liquid and occurs on characteristic time scale t_{α}.

Upon increasing ϕ, the subdiffusive region becomes more pronounced and persists for longer duration, reflecting enhanced caging and slowing of the dynamics.[8,9,42] The upturn in $M(t)$ eventually moves outside of the observation window for $\phi > 0.585$, indicating that the systems behave as glassy solids on the simulated time scales. For a less-confined system ($H = 8.00$), the MSDs also become more subdiffusive as ϕ is increased and are larger at a given ϕ than those measured at $H = 3.00$ (Figure 2(b)).

Similar trends are observed upon decreasing H when the volume fraction is held constant (Figure 3). Interestingly, below a particular value of H, oscillations appear in the subdiffusive caging plateaus ($t \approx 1-10$). These oscillations are not observed in 3D amorphous solids[8,32,43] but have been previously reported in 2D glasses, where they have been interpreted as evidence of LWFs.[30,33,34]

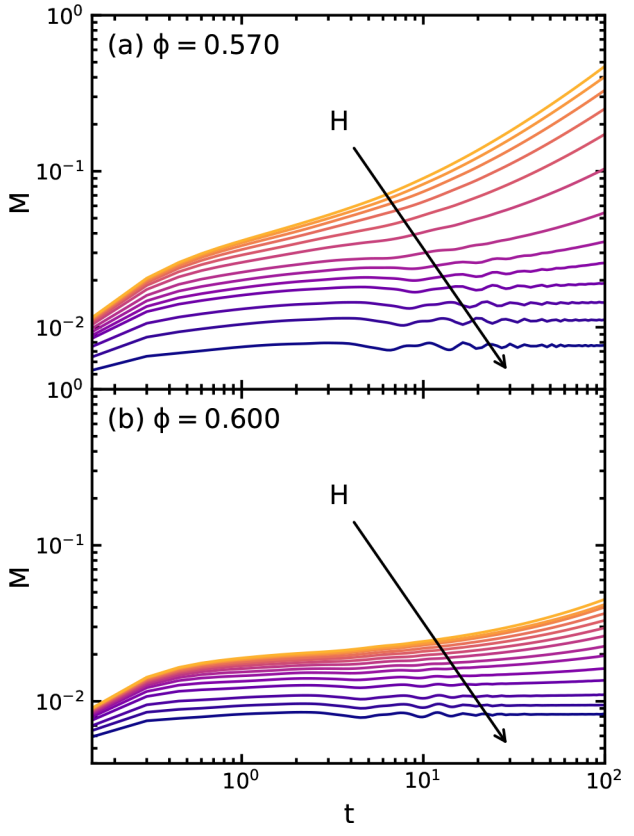

Figure 3. Mean-square displacement $M(t)$ functions for systems with various confinement parameters H and particle volume fractions of (a) $\phi = 0.570$ and (b) $\phi = 0.600$. The arrow indicates the direction of decreasing H. The confinement parameters in (a) are H = 1.00, 1.20, 1.34, 1.70, 2.00, 2.50, 3.00, 4.00, 5.00, 6.00, 7.00, 8.00, 9.00. The confinement parameters in (b) are H = 2.00, 2.50, 3.00, 4.00, 5.00, 6.00, 7.00, 8.00, 9.00, 10.00, 11.00, 12.00, 13.00, 14.00.

Collective Dynamics. In model systems with LWFs, measured properties often depend sensitively on system size due to the artificial suppression of fluctuations larger than the linear dimension L of the periodic simulation cell. Although finite-size effects are generally undesirable, they can be rigorously analyzed to detect and characterize LWFs in model systems.[44,45] Accordingly, we examine the influence of L on $M^{CR}(t)$ and $\Gamma(t)$.

The cage-relative MSD $M^{CR}(t)$ (eq 2) characterizes particle displacements in the reference frame of the center-of-mass of their surrounding nearest neighbors (Figure 4(a)). Hence, it

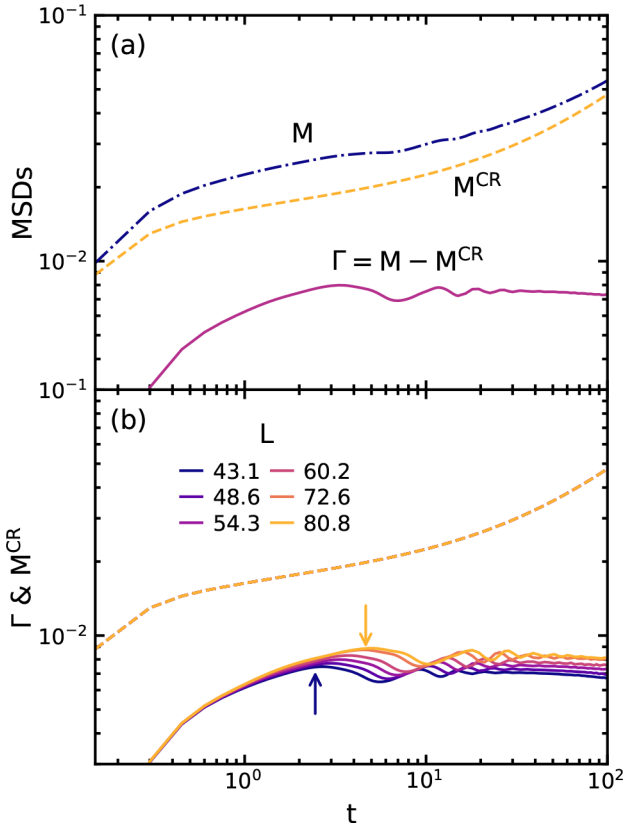

Figure 4. (a) Mean-square displacement $M(t)$, cage-relative MSD $M^{CR}(t)$, and $\Gamma(t) = M(t) - M^{CR}(t)$ for a system with $\{\phi, H\} = \{0.570, 3.00\}$ and periodic edge length $L = 54.3$. (b) $M^{CR}(t)$ and $\Gamma(t)$ for systems with various L and $\{\phi, H\} = \{0.570, 5.00\}$.

describes the cage-rattling dynamics that arise from the relative motion of particles inside their local neighbor cages. We observe that $M^{CR}(t)$ exhibits a crossover from ballistic scaling on short times to diffusive scaling on long times and collapses for all L, indicating that the local dynamics do not exhibit finite-size effects (Figure 4(b)).

By contrast, the contribution remaining after $M^{CR}(t)$ is subtracted from the MSD, $\Gamma(t)$ (eq 4), retains information about collective translational particle motions (Figure 4(a)). This function varies with system size on intermediate time scales, increasing with L for a given observation time t (Figure 4(b)). This system-size dependence indicates the presence of LWFs with characteristic size $>O(L)$.[30,34]

https://doi.org/10.1021/acs.jpcb.2c07417
J. Phys. Chem. B 2023, 127, 961−969

Logarithmically Divergent Fluctuations. Similar finite-size effects are absent in 3D systems but have been observed in 2D solids where they have been attributed to long-wavelength Mermin-Wagner fluctuations.[24,25,28] These LW acoustic modes result in collective translational particle displacements, which are isolated in the function $\Gamma(t)$. Thus, the time scale associated with the local maximum in Γ on intermediate time scales is an estimate of the characteristic time scale t_{LWF} at which LWFs emerge, and the corresponding magnitude $\Gamma(t_{LWF})$ provides an estimate of the squared amplitude of the LWFs.[34]

To determine whether the LWFs observed in our quasi-2D systems are Mermin-Wagner-like, we examine the L-dependence of $\Gamma(t_{LWF})$ for systems with $0.550 \leq \phi \leq 0.600$. Specifically, for an elastic medium, the squared amplitude of the Mermin-Wagner fluctuations diverges logarithmically with system size $A^2 \sim B \log(L)$, where the scaling constant B reflects the elastic contributions to the thermal vibrations and is a function of the shear and bulk moduli of the system.[34] In agreement with this expectation, we observe that the increase in $\Gamma(t_{LWF})$ with L is consistent with logarithmic scaling over distinct ranges of system size and H for each isochore (Figure 5(a,b)), suggesting the presence of MW fluctuations. Further, $\Gamma(t_{LWF})$ varies nonmonotonically with both ϕ (constant H, Figure 5(a)) and H (constant ϕ, Figure 5(b)).

We note that the logarithmic scaling law above is derived in the continuum limit for an elastic medium and hence only valid for the large L (large N) limit. Consequently, deviations are expected in small systems, followed by an eventual crossover to the predicted logarithmic scaling behavior as L becomes sufficiently large. In studies of 2D systems, however, consistency with logarithmic scaling has been observed in systems that are significantly smaller than those examined here.[28,34] Hence, we observe behavior consistent with the logarithmic scaling prediction over the entire range of system sizes examined in our study.

To capture the relationship between the fluctuation magnitude and the confinement, we examine the H-dependence of the logarithmic scaling coefficient B, which for a 2D solid reflects the elastic contributions to the thermal vibrations and is a function of the shear and bulk moduli.[34] For ϕ = 0.570, the elastic coefficient B exhibits a pronounced local maximum at an intermediate H; by contrast, for ϕ = 0.600, B is weakly dependent on H (Figure 6(a)).

We posit that the nonmonotonic variation of both $\Gamma(t_{LWF})$ and B with H for ϕ = 0.570 arises from the competition of two physical processes: changes in local structure driven by increased caging and a transition to 2D-like LWFs as the extent of confinement is increased. In weakly confined systems (large H), particles remain mobile. As a result, when H is large, the local structure is spatially uniform. As H is decreased, the time scale for liquid rearrangement increases, and the time for onset of LWFs t_{LWF} decreases (Figures 3 and 4(b)). These time scales become increasingly separated, and the amplitude of LWFs increases as the system becomes more confined (i.e., more 2D). These factors drive the increases in $\Gamma(t_{LWF})$ and B as H is decreased from the weakly confined regime. For small H, however, confinement drives slowing of dynamics[8] and particles are strongly localized into cages, as in deeply quenched glassy systems.[46−48] In this strongly confined regime, decreasing H reduces variation in local structure due to increasing arrest and hence reduces $\Gamma(t_{LWF})$ and B. Thus, the competition between arrest-driven caging and strengthening

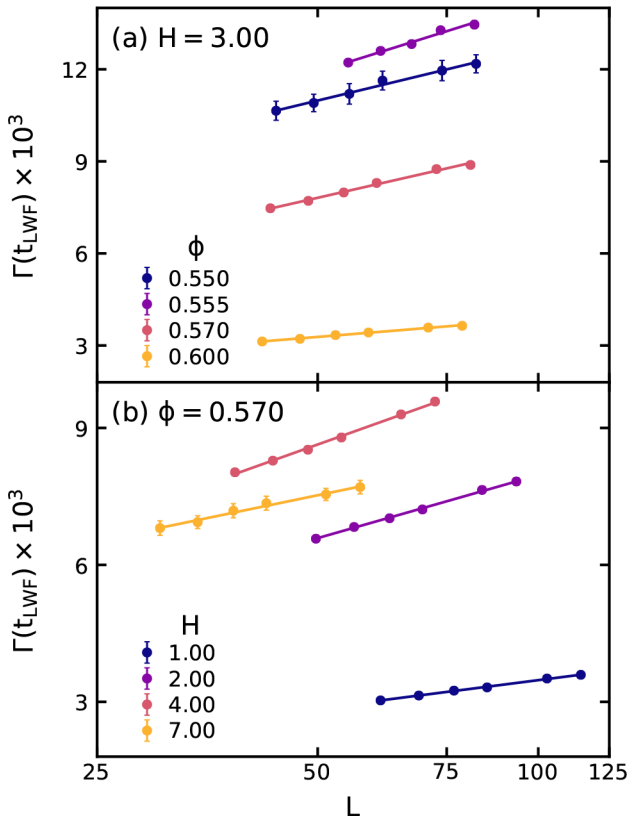

Figure 5. First maximum in $\Gamma \times 10^3$ (i.e., $\Gamma(t_{LWF}) \times 10^3$) as a function of periodic side length L for (a) constant H = 3.00 and (b) constant ϕ = 0.57. At constant H and L, $\Gamma(t_{LWF})$ decreases with increasing ϕ as the system becomes denser. Along an isochore, fluctuations initially increase in magnitude with H as systems become more mobile. Further increases in H, however, lead to a decrease in $\Gamma(t_{LWF})$. The solid lines are logarithmic fits $\Gamma(t_{LWF}) \approx B \log L$ to the data, and data error bars are 95% confidence intervals. From these fits, the coefficient B was extracted, which quantifies how strongly the MW fluctuation magnitude varies with system size.

2D LWFs leads to the local maxima in $\Gamma(t_{LWF})$ and B at an intermediate value of H.

Along the ϕ = 0.600 isochore, by contrast, all samples exhibit glassy dynamics, and the elastic coefficient B is weakly dependent on H. The relatively small change in B with H likely reflects the weaker variation in local structure at higher ϕ due to steric and packing constraints. To distinguish the effects of structure on B and $\Gamma(t_{LWF})$ from those of confinement, we normalized B by a structural metric. To select an appropriate metric, we note that finite variance in the distance between nearest neighbors is a necessary condition to obtain LWFs.[24,25] Further, for 2D crystals, the long-time limit of M^{CR} is twice the variance of the neighbor−neighbor distance.[49,50] We therefore hypothesize that a metric based upon M^{CR} can be used to remove variation in B that arises from local structure. We select as the metric $M^{CR}(t_p)$, where t_p is the time at which M^{CR} attains an inflection point in its caging plateau. This metric is invariant with L and has been associated with cage size in 3D systems.[28,46,47,51,52] Thus, we define a normalized scaling coefficient $B_n = B/M^{CR}(t_p)$.

Along the isochores ϕ = 0.570 and ϕ = 0.600, B_n increases monotonically as H is decreased (Figure 6(b)). This monotonic increase in B_n is expected for a system transitioning from 3D, for which B_n would be effectively zero due to the

https://doi.org/10.1021/acs.jpcb.2c07417
J. Phys. Chem. B 2023, 127, 961−969

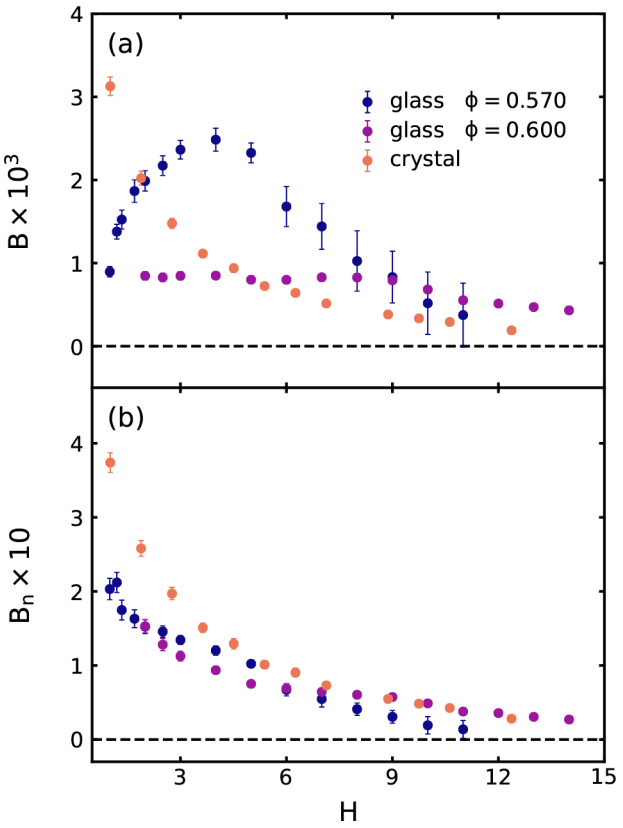

Figure 6. (a) Non-normalized B and (b) normalized B_n scaling coefficients for selected glassy isochores. For comparison, scaling coefficients are also shown for crystalline systems of confined hexagonally close-packed hard spheres. The average particle−particle and particle−wall surface-to-surface separations for the crystalline systems are $1.07\overline{\sigma}$ and constant for all H. The maximum in B for $\phi <$ 0.60 reflects the competition between strengthening LWFs and variation in local structure. The B_n scaling isolates the growth of LWFs relative to variation in local structure.

absence of logarithmic scaling, to 2D LWFs.[24−26] The similarity in the values of B_n for the two ϕ at fixed confinement suggests that normalization by the cage size indeed removes much of the variation in B due to changes in local structure.

To further confirm this idea, we examine the H-dependence of B_n in a system for which the local structure is nearly independent of confinement. To this end, we simulated a series of crystals of hexagonally closed-packed, monodisperse hard spheres confined between two hard walls. The confined crystals are generated such that the average wall−particle and nearest-neighbor separations are $1.07\overline{\sigma}$, which ensures that their local structure and dynamics do not vary significantly with H. For the crystalline systems, the increase of $\Gamma(t_{LWF})$ with L is consistent with logarithmic scaling, indicating that they exhibit LWFs. Both the elastic coefficient B and the normalized coefficient B_n of the crystal systems increase monotonically as H is decreased (Figure 6), as expected for a 3D-to-2D transition in LWFs, and are very close in magnitude. Hence, we conclude that the growth of $\Gamma(t_{LWF})$ with L is indicative of MW fluctuations in quasi-2D confined supercooled liquids and that the nonmonotonic variation of B with H in some samples arises from confinement-induced changes in local structure.

State-Space Dependence. As the confinement length scale H decreases, the nonlocal MW fluctuations are expected to increasingly dominate particle motion. In unconfined 3D geometries, directional correlations between the motions of particles in supercooled liquids and those of their neighbors are small on intermediate to long time scales.[32] By contrast, in a 2D system with LWFs, the displacements of particles are highly directionally correlated with those of the neighbors in their surrounding cage.[32,53] The transition from 3D- to 2D-like dynamics can be characterized by examining the two-particle correlation function $S_{vec,i}$, which quantifies the degree of directional correlation between the displacement of a central particle and those of its surrounding neighbors.[32,40,41] The function $S_{vec,i}$ assumes values of 1 and −1 when the displacement direction and magnitude of the central particle

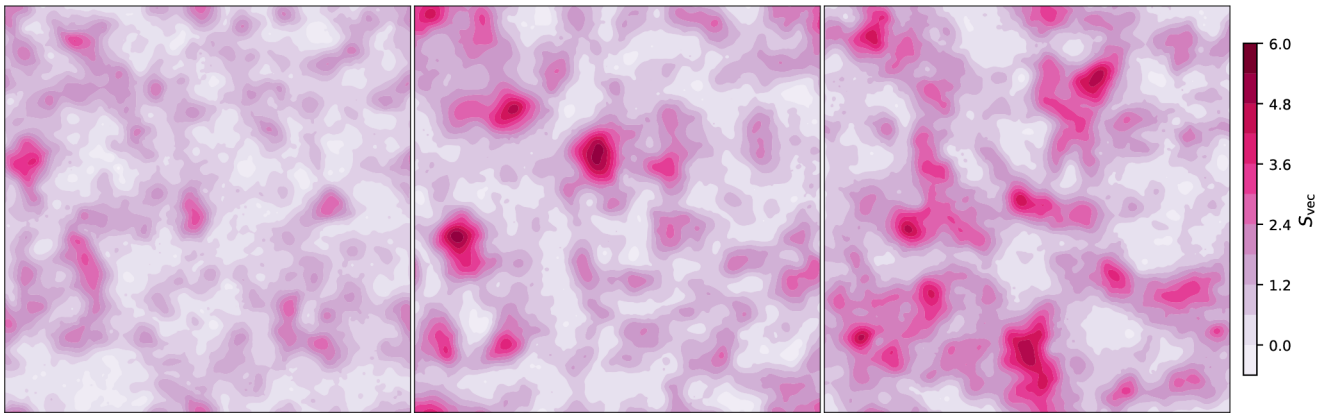

Figure 7. Contour maps of the coarse-grained directional displacement field S_{vec} within the contact layers for systems with approximately the same periodic side length L and cage-relative MSD M^{CR} at the selected lag time but varying levels of confinement H. The constant L controls the maximum possible wavelength of density fluctuations, and the constant M^{CR} controls for variation in local structure. The state points are $\{\phi, H\}$ = (a) {0.59, 13.00}, (b) {0.57, 4.00}, and (c) {0.55, 2.00}. Darkly colored regions in which $S_{vec} \gg 0$ exhibit displacements that are correlated in both direction and magnitude. In brief, S_{vec} is obtained by a sum of Gaussians centered at $\mathbf{r}_i$ that smear the $S_{vec,i}$ of each particle. The maximum value for S_{vec} of 6 reflects the fact that only the Gaussians of the nearest neighbors contribute to the sum. To account for directional correlation alongside significant mobility, the Gaussian variance and height are the MSD and $S_{vec,i}$ of particle i, respectively. The lag time of each displacement is t = 10 simulation time units, which is approximately the time for the first minimum in Γ^{CR}. The extent of spatial correlations decreases with decreasing confinement, i.e., the dark regions are smaller for larger H.

https://doi.org/10.1021/acs.jpcb.2c07417
J. Phys. Chem. B 2023, 127, 961−969

i and all of its nearest neighbors are perfectly correlated and anticorrelated, respectively. To isolate the effects of confinement, we control for variations in local structure by examining three state points with different H but similar L and equal M^{CR} at lag time $t = 10 \approx t_{LW}$.

A weakly confined system ($\{\phi, H\}=\{0.59, 13.00\}$) exhibits modest correlations in directional displacement between neighboring particles (Figure 7). As H is decreased, the correlations become stronger (i.e., S_{vec} increases), and the size of regions of correlated displacement increases. Together, these observations suggest that increasing 2D LWFs in supercooled liquids leads to enhanced collective displacement within regions of particles. This result is consistent with experimental observations of larger displacement correlations in colloids at a 2D oil−aqueous interface compared to 3D systems.[32]

Lastly, to characterize how LWFs vary across the $\{\phi, H\}$ state space, we calculated the elastic coefficient B for supercooled liquids across a range of confinements spanning bulk to quasi-2D systems (Figure 8). LWFs are detectable

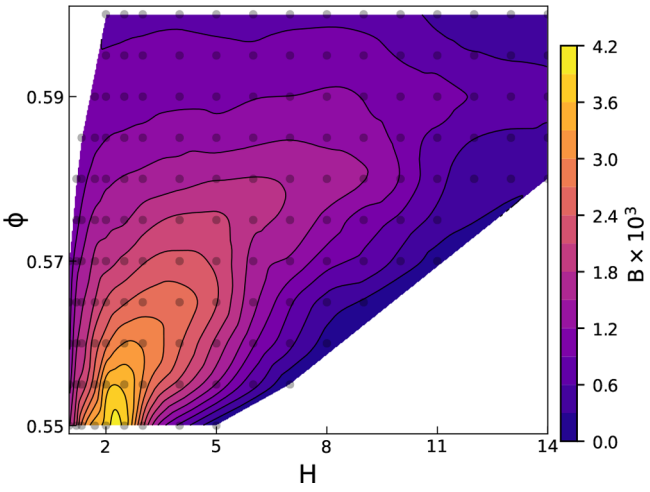

Figure 8. Contour map of the unnormalized scaling coefficient B for varying state point $\{\phi, H\}$, where $0.550 \leq \phi \leq 0.600$ and $1.00 \leq H \leq 14.00$. Contours are generated by local cubic interpolation of B data, and local re-entrance is an artifact of the interpolation. Translucent black dots indicate locations of state points. Values of B have been scaled by a factor of 10^3 for clarity. Nonmonotonic variation of B is more evident for smaller ϕ. LWFs are not detectable via the first maximum in Γ in the white regions of this diagram.

across a broad range of H. As ϕ is increased from 0.550, state points with measurable values of B (by our methods) extend to larger values of H. This result is consistent with the expectation that B (which is a measure of the elastic contributions to the thermal vibrations) should increase as systems become denser and hence more solid-like. Indeed, nonzero values of B are observed up to the largest H studied ($H = 14$) for $\phi \geq 0.580$. For $\phi < 0.580$, our methods fail to detect LWFs beyond $H \approx 10$. We note, however, that 2D LWFs can be present and influence dynamics within normal 2D liquids.[27,54] Thus, alternative approaches may reveal LWFs in more weakly confined systems.

Along isochores with $\phi \leq 0.590$, B attains a maximum at an intermediate value of H (as also seen in Figure 6). This value of B signifies the maximum magnitude of the LWFs induced by finite-size effects. The largest maximum in B occurs at the lowest value of ϕ examined (i.e., in the most liquid-like system). Further, because LWFs are detectable across a narrower range as ϕ is decreased, the change in B with H is steeper. Thus, finite-size effects arising from LWFs are most pronounced for low-ϕ systems in the quasi-2D limit.

While writing this article, Ciamarra and collaborators published a study in which they investigated the change in dynamics for increasingly confined systems containing a 80:20 Kob-Andersen Lennard-Jones glass-forming mixture.[21,55] Using periodic boundary conditions to avoid layering in the confinement direction, they showed that LWFs affected the relaxation dynamics of quasi-2D supercoooled liquid by examining their dependence on lateral size, similar to what is reported here. Further, they compared the time scales associated with structural relaxation and the longest-wavelength vibrational modes and thereby determined whether systems exhibited 2D-like (in which dynamics were dominated by LWFs) or 3D-like (in which dynamics were dominated by structural relaxation) behavior. Interestingly, ref 55 also examined the behavior of the Kob-Andersen mixture confined in a slit geometry, but they did not report observing a nonmonotonic dependence of MW fluctuations on H, as was found in our study. This apparent discrepancy may be due to the fact that the particle volume fraction was not held constant as H was varied in their study nor were the effects of varying ϕ systematically explored. Alternatively, it may arise from the use of different model liquids. In either case, our study presents a complementary analysis of a different model, in which the effects of both particle volume fraction ϕ and the confinement length scale H were systematically explored, revealing distinct behavior in different regions of the parameter space.

Additionally, our analysis of LWFs in the quasi-2D systems is based on global dynamical quantities calculated by averaging over all of the particles in the systems. Nonetheless, the dynamics of confined liquids may be heterogeneous and vary as a function of distance from the bounding walls due to the organization of particles into distinct layers.[16] Thus, we anticipate that additional insights into LWFs in these systems can be obtained by examining the local dynamics in different particle layers. We expect that the dense contact layers start to dominate the average MSD as H is decreased. Indeed, our preliminary examination of local dynamics indicates that long-wavelength MW fluctuations may be enhanced in the dense contact layers near the walls relative to those in the center of the pores, but this topic merits further investigation in future studies. Another promising avenue for future study is the development of structural metrics that provide an improved description of the changes in dynamics observed as the confinement length scale is changed. There has been recent success, for example, in identifying metrics that connect the dynamics of 2D and quasi-2D liquids consisting of bidisperse, nearly hard-sphere particles.[56] Although these structural descriptors do not appear to be directly extensible to polydisperse systems in this study, we anticipate that similar approaches may prove successful in developing metrics that better account for the variations in the strength of the LWFs with confining length scale than those presented here. A second potential structural metric is the hexatic order parameter, which has been shown to describe melting processes[57,58] and nanoparticle adsorption[59] in two dimensions. Our previous computational study showed that the in-plane relaxation time increased exponentially with the correlation length associated with the hexatic order parameter

https://doi.org/10.1021/acs.jpcb.2c07417
J. Phys. Chem. B 2023, 127, 961−969

for confinements whose widths were commensurate with the average particle size.[20] Thus, an interesting avenue for future study is to examine if there is a connection between LWFs and crystalline order.

CONCLUSIONS

Using event-driven molecular dynamics simulations, we showed that confined supercooled liquids exhibit long-wavelength MW fluctuations in the lateral directions parallel to the confining walls, similar to those observed in 2D but not 3D systems. Competition between caging and MW fluctuations as the liquids are increasingly confined leads to a nonmonotonic dependence of the fluctuations on the confinement length scale. Thus, the fluctuation amplitude can be modulated by controlling the particle volume fraction and extent of confinement. The results reveal that LWFs are detectable for volume fractions below random close-packed as long as the confinement is sufficiently strong (in Figure 8); below $\phi < 0.58$, bulk behavior appears for $H > 14$. Thus, choosing $H \gtrsim 20$ appears to be sufficient to avoid LWFs for systems far from random close packing (RCP). For ϕ closer to RCP, however, we are able to detect LWFs even at widths up to $H = 14$, the maximum examined in this study due to the need to simulate systems with large L to determine the scaling behavior. Although their strength appears to decrease as ϕ is increased toward RCP, additional simulations closer to RCP are needed to quantitatively test this speculation.

The detectability of MW fluctuations even in systems where the confinement length scale is an order of magnitude larger than the particle diameter suggests that they may influence the properties of confined liquids in practical settings. Collective displacements in quasi-2D paramagnetic colloids, for example, were found to smear cage rearrangement and enhance particle mobility[53] and to accelerate viscoelastic relaxation and reduce viscosity.[29] Thus, improved understanding of dynamical processes in quasi-2D systems may open new routes to tuning the meso- and macroscopic properties of confined liquids.

AUTHOR INFORMATION

Corresponding Authors

Jeremy C. Palmer − *Department of Chemical and Biomolecular Engineering, University of Houston, Houston, Texas 77204-4004, United States;* orcid.org/0000-0003-0856-4743; Email: jcpalmer@uh.edu

Jacinta C. Conrad − *Department of Chemical and Biomolecular Engineering, University of Houston, Houston, Texas 77204-4004, United States;* orcid.org/0000-0001-6084-4772; Email: jcconrad@uh.edu

Author

Ryan C. Roberts − *Department of Chemical and Biomolecular Engineering, University of Houston, Houston, Texas 77204-4004, United States*

Complete contact information is available at: https://pubs.acs.org/10.1021/acs.jpcb.2c07417

Notes

The authors declare no competing financial interest.

ACKNOWLEDGMENTS

We thank the National Science Foundation (DMR-1904531) and the Welch Foundation (E-1869 and E-1882) for support. Computational resources were generously provided by the Hewlett-Packard Enterprise Data Science Institute at the University of Houston and the Texas Advanced Computing Center at the University of Texas at Austin.

REFERENCES

(1) Gelb, L. D.; Gubbins, K. E.; Radhakrishnan, R.; Sliwinska-Bartkowiak, M. Phase separation in confined systems. *Rep. Prog. Phys.* **1999**, *62*, 1573−1659.

(2) Gubbins, K. E.; Liu, Y.-C.; Moore, J. D.; Palmer, J. C. The role of molecular modeling in confined systems: impact and prospects. *Phys. Chem. Chem. Phys.* **2011**, *13*, 58−85.

(3) Jackson, C. L.; McKenna, G. B. The glass transition of organic liquids confined to small pores. *J. Non-Cryst. Solids* **1991**, *131*−*133*, 221−224.

(4) Noirez, L.; Baroni, P. Identification of a low-frequency elastic behaviour in liquid water. *J. Phys.: Condens. Matter* **2012**, *24*, 372101.

(5) Derjaguin, B.; Bazaron, U.; Zandanova, K.; Budaev, O. The complex shear modulus of polymeric and small-molecule liquids. *Polymer* **1989**, *30*, 97−103.

(6) Keddie, J. L.; Jones, R. A. L.; Cory, R. A. Size-Dependent Depression of the Glass Transition Temperature in Polymer Films. *Europhysics Letters (EPL)* **1994**, *27*, 59−64.

(7) Ellison, C. J.; Torkelson, J. M. The distribution of glass-transition temperatures in nanoscopically confined glass formers. *Nat. Mater.* **2003**, *2*, 695−700.

(8) Nugent, C. R.; Edmond, K. V.; Patel, H. N.; Weeks, E. R. Colloidal glass transition observed in confinement. *Phys. Rev. Lett.* **2007**, *99*, 025702.

(9) Zhang, B.; Cheng, X. Structures and dynamics of glass-forming colloidal liquids under spherical confinement. *Phys. Rev. Lett.* **2016**, *116*, 098302.

(10) Palmer, J. C.; Moore, J. D.; Brennan, J. K.; Gubbins, K. E. Adsorption and diffusion of argon in disordered nanoporous carbons. *Adsorption* **2011**, *17*, 189−199.

(11) Landers, J.; Gor, G. Y.; Neimark, A. V. Density functional theory methods for characterization of porous materials. *Colloids Surf., A* **2013**, *437*, 3−32.

(12) Dobrzanski, C. D.; Gurevich, B.; Gor, G. Y. Elastic properties of confined fluids from molecular modeling to ultrasonic experiments on porous solids. *Appl. Phys. Rev.* **2021**, *8*, 021317.

(13) He, S.; Palmer, J. C.; Qin, G. A non-equilibrium molecular dynamics study of methane transport in clay nano-pores. *Microporous Mesoporous Mater.* **2017**, *249*, 88−96.

(14) Ravinder, R.; Kumar, R.; Agarwal, M.; Krishnan, N. M. A. Evidence of a two-dimensional glass transition in graphene: Insights from molecular simulations. *Sci. Rep.* **2019**, *9*, 4517.

(15) Van Winkle, D. H.; Murray, C. A. Layering in colloidal fluids near a smooth repulsive wall. *J. Chem. Phys.* **1988**, *89*, 3885−3891.

(16) Mittal, J.; Truskett, T. M.; Errington, J. R.; Hummer, G. Layering and Position-Dependent Diffusive Dynamics of Confined Fluids. *Phys. Rev. Lett.* **2008**, *100*, 145901.

(17) Pieranski, P.; Strzelecki, L.; Pansu, B. Thin Colloidal Crystals. *Phys. Rev. Lett.* **1983**, *50*, 900−903.

(18) Schmidt, M.; Löwen, H. Freezing between Two and Three Dimensions. *Phys. Rev. Lett.* **1996**, *76*, 4552−4555.

(19) Mandal, S.; Lang, S.; Gross, M.; Oettel, M.; Raabe, D.; Franosch, T.; Varnik, F. Multiple reentrant glass transitions in confined hard-sphere glasses. *Nat. Commun.* **2014**, *5*, 4435.

(20) Roberts, R. C.; Marioni, N.; Palmer, J. C.; Conrad, J. C. Dynamics of polydisperse hard-spheres under strong confinement. *Mol. Phys.* **2020**, *118*, e1728407.

(21) Kob, W.; Andersen, H. C. Testing mode-coupling theory for a supercooled binary Lennard-Jones mixture I: The van Hove correlation function. *Phys. Rev. E* **1995**, *51*, 4626−4641.

(22) Gebremichael, Y.; Vogel, M.; Glotzer, S. Particle dynamics and the development of string-like motion in a simulated monoatomic supercooled liquid. *J. Chem. Phys.* **2004**, *120*, 4415−4427.

(23) Flenner, E.; Szamel, G. Fundamental differences between glassy dynamics in two and three dimensions. *Nat. Commun.* **2015**, *6*, 7392.
(24) Mermin, N. D.; Wagner, H. Absence of ferromagnetism or antiferromagnetism in one-or two-dimensional isotropic Heisenberg models. *Phys. Rev. Lett.* **1966**, *17*, 1133−1136.
(25) Mermin, N. D. Crystalline order in two dimensions. *Phys. Rev.* **1968**, *176*, 250−254.
(26) Kosterlitz, J. M.; Thouless, D. J. Ordering, metastability and phase transitions in two-dimensional systems. *Journal of Physics C: Solid State Physics* **1973**, *6*, 1181−1203.
(27) Li, Y.-W.; Mishra, C. K.; Sun, Z.-Y.; Zhao, K.; Mason, T. G.; Ganapathy, R.; Pica Ciamarra, M. Long-wavelength fluctuations and anomalous dynamics in 2-dimensional liquids. *Proc. Natl. Acad. Sci. U. S. A.* **2019**, *116*, 22977−22982.
(28) Illing, B.; Fritschi, S.; Kaiser, H.; Klix, C. L.; Maret, G.; Keim, P. Mermin−Wagner fluctuations in 2D amorphous solids. *Proc. Natl. Acad. Sci. U. S. A.* **2017**, *114*, 1856−1861.
(29) Flenner, E.; Szamel, G. Viscoelastic shear stress relaxation in two-dimensional glass-forming liquids. *Proc. Natl. Acad. Sci. U.S.A.* **2019**, *116*, 2015−2020.
(30) Shiba, H.; Kawasaki, T.; Kim, K. Local Density Fluctuation Governs the Divergence of Viscosity Underlying Elastic and Hydrodynamic Anomalies in a 2D Glass-Forming Liquid. *Phys. Rev. Lett.* **2019**, *123*, 265501.
(31) Zhang, B.; Cheng, X. Long-wavelength fluctuations and static correlations in quasi-2d colloidal suspensions. *Soft Matter* **2019**, *15*, 4087−4097.
(32) Vivek, S.; Kelleher, C. P.; Chaikin, P. M.; Weeks, E. R. Long-wavelength fluctuations and the glass transition in two dimensions and three dimensions. *Proc. Natl. Acad. Sci. U. S. A.* **2017**, *114*, 1850−1855.
(33) Shiba, H.; Yamada, Y.; Kawasaki, T.; Kim, K. Unveiling dimensionality dependence of glassy dynamics: 2D infinite fluctuation eclipses inherent structural relaxation. *Phys. Rev. Lett.* **2016**, *117*, 245701.
(34) Shiba, H.; Keim, P.; Kawasaki, T. Isolating long-wavelength fluctuation from structural relaxation in two-dimensional glass: Cage-relative displacement. *J. Phys.: Condens. Matter* **2018**, *30*, 094004.
(35) Tarjus, G. Glass transitions may be similar in two and three dimensions, after all. *Proc. Natl. Acad. Sci. U. S. A.* **2017**, *114*, 2440−2442.
(36) Bannerman, M. N.; Sargant, R.; Lue, L. DynamO: a free O(N) general event-driven molecular dynamics simulator. *J. Comp. Chem.* **2011**, *32*, 3329−3338.
(37) Grigera, T. S.; Parisi, G. Fast Monte Carlo algorithm for supercooled soft spheres. *Phys. Rev. E* **2001**, *63*, 045102.
(38) Berthier, L.; Charbonneau, P.; Jin, Y.; Parisi, G.; Seoane, B.; Zamponi, F. Growing timescales and lengthscales characterizing vibrations of amorphous solids. *Proc. Natl. Acad. Sci. U. S. A.* **2016**, *113*, 8397−8401.
(39) Ninarello, A.; Berthier, L.; Coslovich, D. Models and algorithms for the next generation of glass transition studies. *Phys. Rev. X* **2017**, *7*, 021039.
(40) Weeks, E. R.; Crocker, J. C.; Weitz, D. A. Short-and long-range correlated motion observed in colloidal glasses and liquids. *J. Phys.: Condens. Matter* **2007**, *19*, 205131.
(41) Doliwa, B.; Heuer, A. Cooperativity and spatial correlations near the glass transition: Computer simulation results for hard spheres and disks. *Phys. Rev. E* **2000**, *61*, 6898−6908.
(42) Edmond, K. V.; Nugent, C. R.; Weeks, E. R. Influence of confinement on dynamical heterogeneities in dense colloidal samples. *Phys. Rev. E* **2012**, *85*, 041401.
(43) Berthier, L.; Kob, W. The Monte Carlo dynamics of a binary Lennard-Jones glass-forming mixture. *J. Condens. Matter Phys.* **2007**, *19*, 205130.
(44) Binder, K. Critical Properties from Monte Carlo Coarse Graining and Renormalization. *Phys. Rev. Lett.* **1981**, *47*, 693−696.
(45) Binder, K. Theory of first-order phase transitions. *Rep. Prog. Phys.* **1987**, *50*, 783−859.
(46) Hung, J.-H.; Patra, T. K.; Meenakshisundaram, V.; Mangalara, J. H.; Simmons, D. S. Universal localization transition accompanying glass formation: insights from efficient molecular dynamics simulations of diverse supercooled liquids. *Soft Matter* **2019**, *15*, 1223−1242.
(47) Larini, L.; Ottochian, A.; De Michele, C.; Leporini, D. Universal scaling between structural relaxation and vibrational dynamics in glass-forming liquids and polymers. *Nat. Phys.* **2008**, *4*, 42−45.
(48) Starr, F. W.; Sastry, S.; Douglas, J. F.; Glotzer, S. C. What do we learn from the local geometry of glass-forming liquids? *Phys. Rev. Lett.* **2002**, *89*, 125501.
(49) Zahn, K.; Lenke, R.; Maret, G. Two-stage melting of paramagnetic colloidal crystals in two dimensions. *Phys. Rev. Lett.* **1999**, *82*, 2721−2724.
(50) Zahn, K.; Maret, G. Dynamic criteria for melting in two dimensions. *Phys. Rev. Lett.* **2000**, *85*, 3656−3659.
(51) Simmons, D. S.; Cicerone, M. T.; Zhong, Q.; Tyagi, M.; Douglas, J. F. Generalized localization model of relaxation in glass-forming liquids. *Soft Matter* **2012**, *8*, 11455−11461.
(52) Charbonneau, P.; Ikeda, A.; Parisi, G.; Zamponi, F. Dimensional study of the caging order parameter at the glass transition. *Proc. Natl. Acad. Sci. U. S. A.* **2012**, *109*, 13939−13943.
(53) Mazoyer, S.; Ebert, F.; Maret, G.; Keim, P. Dynamics of particles and cages in an experimental 2D glass former. *EPL (Europhysics Letters)* **2009**, *88*, 66004.
(54) Li, Y.-W.; Li, Z.-Q.; Hou, Z.-L.; Mason, T. G.; Zhao, K.; Sun, Z.-Y.; Pica Ciamarra, M. Dynamics in two-dimensional glassy systems of crowded Penrose kites. *Phys. Rev. Mater.* **2019**, *3*, 125603.
(55) Yang, J.; Li, Y.-W.; Ciamarra, M. P. Long-wavelength fluctuations and dimensionality crossover in confined liquids. *Phys. Rev. Res.* **2021**, *3*, 033172.
(56) Tian, J.; Kob, W.; Barrat, J.-L. Are strongly confined colloids good models for two dimensional liquids? *J. Chem. Phys.* **2022**, *156*, 164903.
(57) Bernard, E. P.; Krauth, W. Two-step melting in two dimensions: first-order liquid-hexatic transition. *Phys. Rev. Lett.* **2011**, *107*, 155704.
(58) Engel, M.; Anderson, J. A.; Glotzer, S. C.; Isobe, M.; Bernard, E. P.; Krauth, W. Hard-disk equation of state: First-order liquid-hexatic transition in two dimensions with three simulation methods. *Phys. Rev. E* **2013**, *87*, 042134.
(59) Schwenke, K.; Isa, L.; Del Gado, E. Assembly of Nanoparticles at Liquid Interfaces: Crowding and Ordering. *Langmuir* **2014**, *30*, 3069−3074.

https://doi.org/10.1021/acs.jpcb.2c07417
J. Phys. Chem. B 2023, 127, 961−969